analytical chemistry

Article

Cite This: Anal. Chem. 2019, 91, 12055−12062

pubs.acs.org/ac

H_2-Based Electrochemical Biosensor with Pd Nanowires@ZIF-67 Molecular Sieve Bilayered Sensing Interface for Immunoassay

Shuzhen Lv,[†] Kangyao Zhang,[†] Ling Zhu,[†] Dianping Tang,*[,†] Reinhard Niessner,[‡] and Dietmar Knopp*[,‡]

[†]Key Laboratory of Analytical Science for Food Safety and Biology (MOE & Fujian Province), Department of Chemistry, Fuzhou University, Fuzhou 350108, People's Republic of China

[‡]Chair for Analytical Chemistry and Water Chemistry, Institute of Hydrochemistry, Technische Universität München, Marchioninistrasse 17, München D-81377, Germany

Supporting Information

ABSTRACT: With the introduction of gas-based contactless electrochemical biosensors lies the prospects of separating the sensing interface from the bioassembly platform, enhancing stability, and exploring signal transduction mechanism, all intimately linking to development of immunoassay. Herein, we report on a H_2-based electrochemical biosensor whose signals derived from the chemical signal transduction between a H_2 and Pd nanowires@ZIF-67 (ZIF: Zeolitic Imidazolate Frameworks) bilayered sensing interface for immunoassay. Dendritic Pt nanoparticles (DPNs) conjugated on the detection antibody were introduced on the interface of a magnetic microsphere according to an immune sandwich assembly between the antigen and antibody. H_2 as a bridge originates from DPNs catalyzing NH_3BH_3 and links biological signals to electrical signals by reacting with Pd nanowires. Nevertheless, the response of Pd nanowires being extremely effected by O_2 in air due to the competitive adsorption on the surface of Pd nanostructures as well as the reaction between chemisorbed O (Pd−O) and adsorbed dihydrogen lead to a decrease in H absorption into PdH_x and poor sensing responses under low target concentration. Porous ZIF-67 (window aperture 0.331 nm) as a molecular sieve self-assembling on the surface of the Pd nanowires film could easily permeate H_2 (kinetic diameter of 0.289 nm), while interferential O_2 (kinetic diameter of 0.346 nm) has difficultly passing through the ZIF-67 layer to contact Pd nanowires and achieves a response of a lower concentration target as well as faster response rate. Under optimal conditions, H_2-based electrochemical biosensors exhibit great response toward target alpha-fetoprotein (AFP) within a dynamic working range of 0.1−50 ng mL^{-1} at a detection limit of 0.04 ng mL^{-1}. Our strategy provides a reusable sensing interface, high specificity, and acceptable accuracy for the immunoassay. In addition, it also expands a promising platform for application as a molecular sieve in electrochemical biosensors.

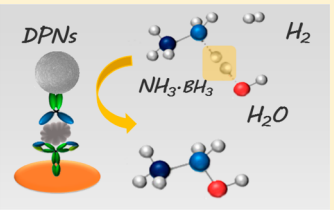

Gas-based contactless electrochemical biosensors, compared with traditional electrochemical biosensors, can separate the sensing interface from the bioassembly platform, get rid of the tedious reconstruction process, accomplish a reusable sensing interface, and enhance the precision, stability, and reproducibility of the detection results. Signal transduction in gas-based electrochemical biosensors explored in the past years can be divided into physical and chemical signal transduction according to the different mechanism of electrical signal generation. Specifically, the biological signals generated by the biorecognition present in the form of a quantified gas, indirectly converting into an electrical signal according to physical and chemical response between the gas and electrode interface materials. Physical signal transduction is generally accompanied by the deformation of flexible electrode material or changes in electrode contact areas due to the increased pressure of the detection system with the generated gas, resulting in the generation of electrical signals.[1,2] On the other hand, the chemical signal transduction mechanism in the developed gas-based electrochemical biosensor usually originates from the redox reactions between gas and interface materials (e.g., metal-oxide semiconductor) on the electrodes. The increase or decrease in an electrical signal depends on the redox properties of the as-produced gas (oxidizing gas, reducing gas, etc.) and the difference in electron and hole density of various semiconductors.[3−6]

Hydrogen (H_2) as a reducing gas can react with oxygen ions (O_2^-) on the surface of metal-oxide semiconductors leading to changes in the conductivity; however, the high sensing temperature required for the chemical reaction restrains the applications for the electrochemical biosensors.[7] Specially, H_2 sensors based on Pd nanostructures have been heavily studied by many researchers for their advantages of simplicity and low power consumption. H_2 can dissociate from molecular hydrogen by absorbing and dissolve into palladium (Pd) to form PdH_x, causing an increase in the resistance of Pd at room temperature.[8] Therefore, Pd nanostructures exhibiting prominent advantages of low detection temperature, regulated conductivity, and low cost are employed in H_2-based electrochemical biosensors.[3] However, inherent limitations

Received: July 13, 2019
Accepted: August 22, 2019
Published: August 22, 2019

DOI: 10.1021/acs.analchem.9b03177
Anal. Chem. 2019, 91, 12055−12062

Scheme 1. Illustration of H_2-Based Electrochemical Biosensor with Pd Nanowires@ZIF-67 Molecular Sieve Bilayered Sensing interfaces: (A) Interaction between Pd Nanowires and H_2 under O_2 Interference. (B) Self-Assembly ZIF-67 on Surface of Pd Nanowires Films as Molecular Sieve Excluding O_2 Interference

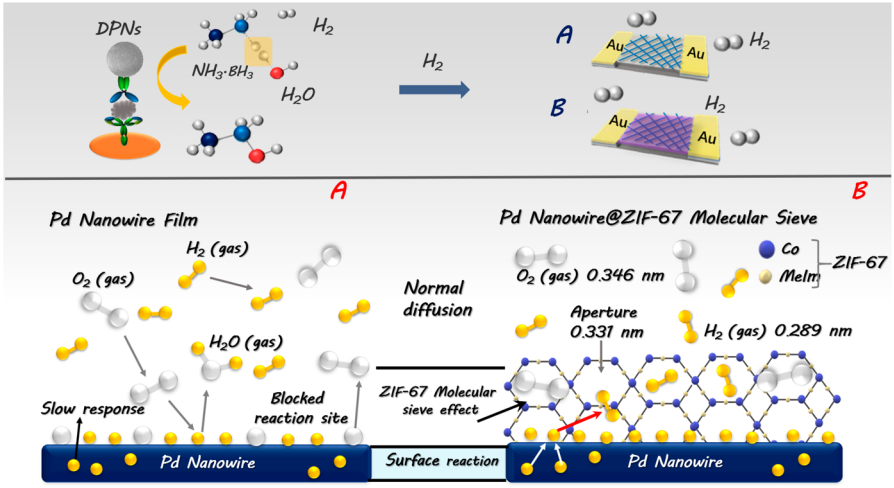

appear when interferential oxygen exists in the biosensing detection system. The inextricable oxygen adsorbed on the surface of Pd nanostructures can occupy the adsorption site of hydrogen; futhermore, the chemisorbed O (Pd−O) combines with adsorbed dihydrogen dissociating from hydrogen to generate water, leading to less PdH_x and poor sensing responses under low hydrogen concentration.[9] Therefore, constructing a sensing platform to block oxygen and only make hydrogen contact with Pd nanostructures are necessary.

ZIFs (Zeolitic Imidazolate Frameworks) are ascribed to a subfamily of a metal−organic framework (MOF) with strong coordination between imidazolate and metal ions encouraging the structural integrity to be fairly stable even in water.[10] The excellent chemical stability and famed crystalline pore structures as well as high surface areas of ZIFs are widely explored in the fields of sensors, catalysis, and gas separation.[11−13] Highly porous structures of ZIFs enhancing gas preconcentration and achieving gas selectivity by adjusting pore aperture diameter are good candidates for gas separation as molecular sieves.[14−17] The ideal MOF molecular sieve films with appropriate window apertures on the surface of sensing interfaces in H_2-based electrochemical biosensors can easily permeate H_2, while the interference gases are excluded. ZIF-67 ($[Co\text{-}(MeIm)_2]_n$) (MeIm = methylimidazole) possessing an isostructural SOD zeolitic topology with a window aperture of 0.331 nm has been applied for gas separation.[18,19] In the process of hydrogen separation, ZIF-67 allows H_2 (kinetic diameter of 0.289 nm) to penetrate, whereas larger gas molecules (>0.33 nm) cannot. Compared with the most attractive ZIF-8, they are isostructural,[20] but the aperture of ZIF-67 (3.31 Å) is smaller than ZIF-8 (3.42 Å). The tighter structure as well as narrower aperture makes for a better hydrogen separation effect.[21] Hence, ZIF-67 as a molecular sieve to exclude interference gas such as O_2 (kinetic diameter of 0.346 nm) in H_2-based electrochemical biosensors with Pd nanostructures is promising.

In our strategy, H_2-based electrochemical biosensors through chemical signal transduction between H_2 and Pd nanowires, assisted by ZIF-67 ($[Co(MeIm)_2]_n$) molecular sieve films, are constructed by nonenzymatic assembly of immunoreagents for cancer biomarker detection. Alpha-fetoprotein (AFP, as the model analyte in this work) is one of the most extensively explored tumor-associated glycoproteins, closely related to clinical hepatocellular cancer (HCC), yolk sac tumor, and other diseases.[22−24] The significance of AFP testing lies in early diagnosis for timely treatment as well as judgment of postoperative recovery. As shown in Scheme 1, the immunochemical identification of AFP at the interface of magnetic beads modified with streptavidin introduces dendritic Pt nanoparticles (DPNs) that catalyze dehydrogenation of NH_3BH_3 to produce H_2[25] into the airtight detection system according to Ab_2@DPNs assembly and antigen−antibody recognition. As for the sensing interface, ZIF-67 (micropores size 0.331 nm) self-assembled on the surface of the Pd nanowires film is selected as the molecular sieve to exclude O_2 (kinetic diameter of 0.346 nm), permeate H_2 (kinetic diameter of 0.289 nm), and guarantee as much PdH_x generation as possible. Due to the interception of ZIF-67, O_2 neither adsorbed on the Pd nanowires to occupy H_2 adsorption sites nor formed chemisorbed O to react with adsorbed dihydrogen (Pd−O + 3/2H (ads) → Pd−H + H_2O (ads); H_2O (ads) → H_2O (gas)),[9,26] leading to an increase in H absorption into PdH_x, achieving a response of lower concentration AFP, faster response speed, and better selectivity.

EXPERIMENTAL SECTION

Material and Reagent. Hexachloroplatinic (IV) acid hexahydrate ($H_2PtCl_6{\cdot}6H_2O$), L-ascorbic acid (AA), sodium carbonate (Na_2CO_3), disodium hydrogen phosphate dodecahydrate ($Na_2HPO_4{\cdot}12H_2O$), potassium phosphate monobasic (KH_2PO_4), sodium chloride (NaCl), bovine serum albumin (BSA), sodium azide (NaN_3), sodium hydroxide (NaOH), sodium iodide (NaI), palladium chloride ($PdCl_2$), polyvinylpyrrolidone (K30), and streptavidin-functionalized magnetic beads (MBs) were acquired from Aladdin (Shanghai, China). Streptavidin magnesphere paramagnetic particles (PMPs), α-fetoprotein (AFP), and monoclonal biotin-anti-AFP antibody (Ab_1) were purchased from Cellwaylab (Henan, China). Polyclonal anti-AFP antibody (Ab_2) was aquired from BiosPacific, Inc. (CA, USA). A human AFP enzyme-linked immunosorbent assay (ELISA) kit was purchased from Biocell Biotechnol., Inc. (Zhengzhou, China). Ultrapure water derived

DOI: 10.1021/acs.analchem.9b03177
Anal. Chem. 2019, 91, 12055−12062

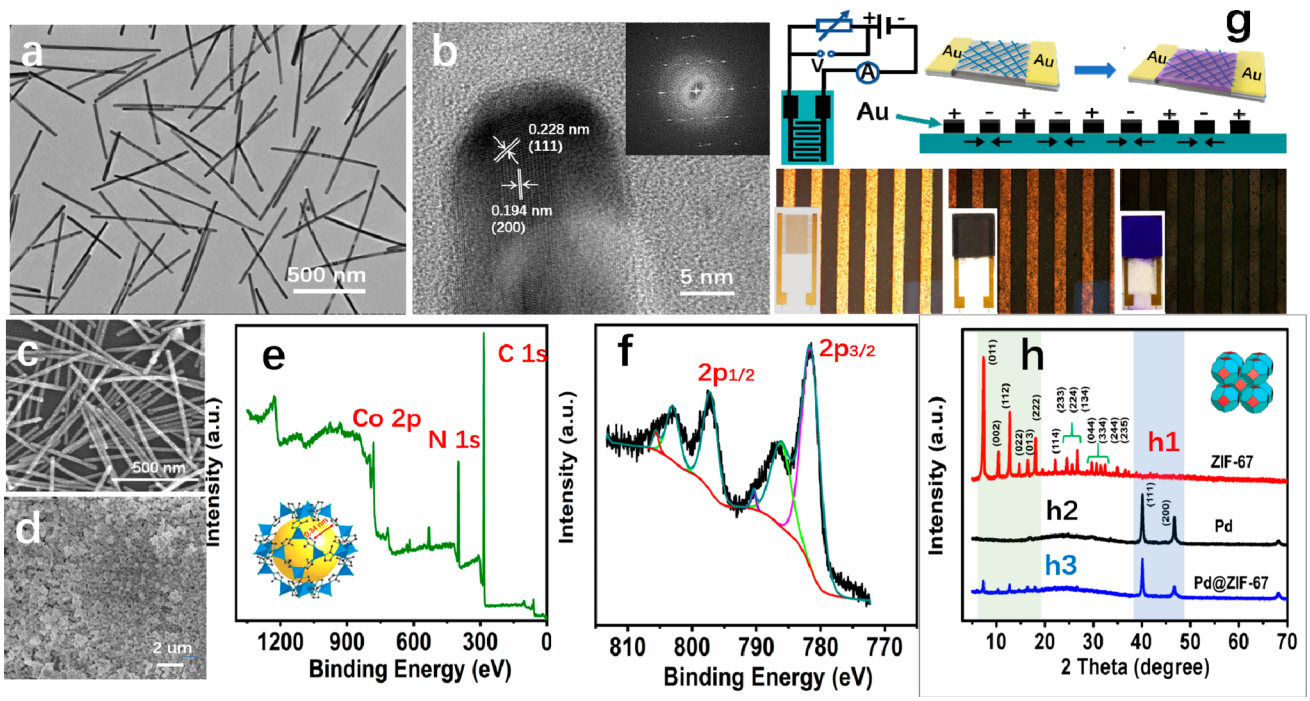

Figure 1. (a) TEM and (b) HRTEM images of Pd nanowires (insert: selected-area-electron diffraction patterns of individual nanowires). SEM images of (c) pristine Pd nanowires and (d) self-assembly ZIF-67 on the surface of Pd nanowires. (e) Full XPS spectrum of ZIF-67; high-resolution XPS spectrum of (f) Co 2p. (g) Surface micrographs of Au interdigital electrode, Au interdigital electrode coated with Pd nanowires, and Au interdigital electrode coated with Pd nanowires@ZIF-67 (from left to right). (h) XRD patterns of (h1) ZIF-67, (h2) Pd nanowires, and (h3) Pd nanowires@ZIF-67.

from a Millipore water purification system (18.2 MΩ cm, Milli-Q, Millipore) was used throughout all experiments.

Construction of Pd Nanowires@ZIF-67 Sensing Interface. Prior to constructing a sensing platform, Pd nanowires were prepared by one-pot synthesis according to a previous method with minor modification.[27] $PdCl_2$ (17.7 mg) and NaI (300 mg) were dissolved into 24 mL of an aqueous solution containing 800 mg of PVP (MW = 30,000). The mixture was continuously stirred until the solution turned a homogeneous dark red. Then, the dark red solution was transferred into a 20 mL Teflon-lined stainless-steel autoclave and heated at 200 °C for 4 h. After the temperature cooled to room temperature, the products were obtained by precipitation with isopropanol and centrifugation at 7180*g*. The products were washed twice with an ethanol−isopropanol mixture and purified by water three times.

Then, the Pd nanowires thin-film which coated the interdigital electrode was fabricated by dipping technology. The gold-plated interdigital electrodes, which consisted of 37 pole-pairs, with lengths of 2 cm and widths of 1 cm (thickness: 0.5 mm), were cleaned with water and acetone in turn. The dry electrodes were immersed into the Pd nanowires solution (10 mL, 0.5 mg mL^{-1}) and upward vertically lifted from the solution at a speed of 500 nm s^{-1} at room temperature (RT).

Finally, the Pd nanowires@ZIF-67 sensing interfaces were fabricated by ZIF-67 self-assembly on the surface of Pd nanowires thin films on gold-plated interdigital electrodes. The as-prepared electrodes were infiltrated into 30 mL of the precursor solution containing 297 mg of $Co(NO_3)_2{\cdot}6H_2O$ and 328.5 mg of 2-methylimidazole for growth of ZIF-67.[28] The various self-assembly times (1−6 h) formed different thicknesses of Pd nanowires@ZIF-67 films. Then, the electrodes were taken out from the reaction solution, washed with water to remove excess ligand and ions, and dried at RT for future use.

Preparation of Dendritic Pt Nanoparticles (DPNs) and Ab_2@DPNs Assembly. Dendritic Pt nanoparticles (DPNs) were synthesized by a rapid and one-step method according to a previous report with minor modification.[29] In a typical synthesis, 35.2 mg of ascorbic acid was dissolved into 19.22 mL of H_2O; then, 980 μL of H_2PtCl_6 (2%) and 30 μL of NaOH (5 M) were dropped into the solution in turn. The mixture was heated in a water bath at 60 °C for different times (3, 5, 7, 10 min). Finally, brown monodisperse DPNs were obtained.

The anti-human AFP detection antibody (anti-AFP DAb) conjugated DPNs (Ab_2@DPNs) were prepared on the basis of our previously reported method.[30] Initially, the pH of DPNs (3.0 mL) was adjusted to 9.0 by a Na_2CO_3 (0.1 M) aqueous solution. Following that, 15 μL of Ab_2 (5 mg mL^{-1}) was dropped into the DPNs solution, and the mixture was shaken for 0.5 h at RT. Then, the mixture was incubated at 4 °C in a refrigerator overnight. Finally, 300 μL of blocking solution (5% BSA) was added into the above solution. After 40 min of incubation, the final Ab_2@DPNs were collected by centrifugation (13,000*g*, 4 °C, 15 min), washed with PBS (pH 7.4), and redispersed in 1.0 mL of PBS solution (0.05% NaN_3, 0.5% Tween 20, 1.0% BSA, pH 7.4) for future use.

Construction of H_2-Based Electrochemical Biosensor. First, the antibody-conjugated magnesphere paramagnetic particles (PMPs) were prepared according to streptavidin−biotin combination. The purchased streptavidin-modified PMPs (1.0 mg mL^{-1}) were washed by a PBS buffer (1.0 mM, 0.05% Tween-20, pH 7.4) and then dispersed in a 1.0 mM PBS solution. The biotin-AFP monoclonal antibodies (5.0 mg mL^{-1}) were mixed with PMPs with slight shaking for 60 min at RT. Due to the specific identification between biotin

DOI: 10.1021/acs.analchem.9b03177
Anal. Chem. 2019, 91, 12055−12062

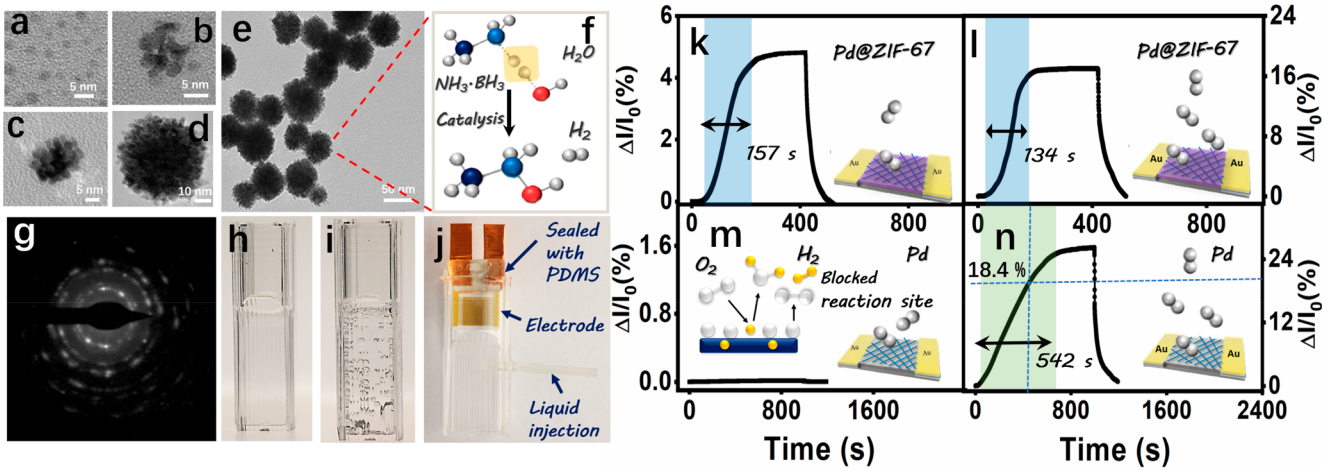

Figure 2. (a–e) TEM images of DPNs at different reaction times: (a) 3 min, (b) 5 min, (c) 7 min, (and d, e) 10 min, respectively. (g) Corresponding SAED pattern of (d) single DPN. (f) Schematic of DPNs catalyzing NH_3BH_3 to produce H_2. Photographs of characteristics of H_2 gas bubbles from NH_3BH_3 aqueous solution before (h) and after (i) the addition of DPNs. (j) Photographs of sensing device. Responses of (k, l) Pd nanowires @ZIF-67 and (m, n) Pd nanowires at the AFP concentrations of (k, m) 2.0 ng mL^{-1} and (l, n) 50 ng mL^{-1}, respectively.

and streptavidin, antibody-conjugated PMPs were obtained. After magnetic separation, the results were resuspended into 0.5 mL of PBS (pH 7.4) containing 1.0 wt % BSA and stored at 4 °C for further use.

The immunoassay was carried out in 0.5 mL centrifuge tubes by addition of 50 μL of AFP standards or samples with various concentrations and 50 μL of the prepared antibody-conjugated PMPs suspension. After incubation for 1 h at 37 °C, the obtained immune mixture was washed with PBS by magnetic separation, followed by the addition of 100 μL of the prepared Ab_2@DPNs and incubated for an additional 50 min under the same condition. The formed immunocomplex was purified by magnetic separation again and washed as before. Subsequently, the immunocomplex was transferred into the detection cell to catalyze dehydrogenation of ammonia borane (0.5 mg mL^{-1}). Meanwhile, at the top of the airtight detection cell, the prepared gold interdigital electrode coated on the Pd nanowires@ZIF-67 thin film was connected with a CHI850D electrochemical workstation to record the changes in current under different target concentrations. The electrochemical biosensor response (R) was defined as $R = (I_0 - I_g)/I_0$ (%) (I_0 stands for the steady-state baseline current, and I_g is on behalf of the current at different concentrations of the target). Response time was the time required for the $0.9\Delta R_{max}$ response after interacting with H_2, and the recovery time was defined as the time for $0.1\Delta R_{max}$ after exposure to the air.

RESULTS AND DISCUSSION

Characterization of Pd Nanowires@ZIF-67. The representative transmission electron microscopy (TEM) images of the as-prepared Pd nanowires are shown in Figure 1a. The nanowires with dominant form had a uniform diameter around 15 nm along their total length, which could be up to the range of 1.0–1.5 μm. Including all of the Pd nanowires, two kinds of lattice fringes with 0.228 and 0.194 nm interplanar spacings, attributed to {111} and {200} planes of fcc Pd, were presented in a characteristic high resolution TEM (HRTEM) image (Figure 1b). The electron diffraction patterns inserted in Figure 1b indicated the single crystal state of palladium nanowires. The morphology features of the Pd nanowires (Figure 1c) as well as the self-assembly surface architecture of ZIF-67 on the surface of the nanowires were investigated by scanning electron microscopy (SEM). It could be clearly observed that ZIF-67 films completely covered the Pd nanowires films (Figure 1d) on silicon wafers after self-assembly. The major elements were further confirmed by X-ray photoelectron spectroscopy (XPS). The peaks at 334.2 and 339.4 eV were attributed to Pd $3d_{5/2}$ and $3d_{3/2}$, respectively according to the high-resolution XPS spectrum of Pd 3d, indicating Pd^0 (Figure S1). Figure 1e reveals the full survey spectrum of the ZIF-67 films on the surface of the Pd nanowires with elements of Co, N, and C. For the high-resolution spectrum of Co 2p (Figure 1f), two main peaks located at 797.1 and 781.5 eV were assigned to Co $2p_{1/2}$ and Co $2p_{3/2}$, respectively.[31] The corresponding satellite binding energies of the Co $2p_{3/2}$ main peak were at about 786.2 and 790.4 eV. Therefore, Co(II) was the main form existing in the self-assembly ZIF-67 film. Moreover, the Pd nanowires @ZIF-67 architecture structure was further demonstrated by X-ray diffraction (XRD) in the 2θ range from 5° to 70° at a scanning rate of 15° min^{-1}. As depicted in Figure 1h, the diffraction peaks of Pd nanowires alone (curve h2) were in accordance with standard Pd (JCPDS No. 16-0334), and the overall structure remained unchanged after the ZIF-67 films were coated on the surface of it. On the other hand, the XRD patterns of Pd nanowires@ZIF-67 (curve h3) matched well with the simulated ZIF-67[32] demonstrating the ZIF-67 architecture structure. Finally, micrographs of the gold interdigital electrode before and after coating the Pd nanowires film as well as Pd nanowires@ZIF-67 film are shown in Figure 1g. The color of the Pd nanowires-coated gold interdigital electrode changed from blank to blue after ZIF-67 self-assembly.

Feasibility of H_2-Based Electrochemical Biosensor for AFP Detection. In our strategy, the electrochemical signals were originated from the reaction of Pd nanowires@ZIF-67 films and H_2 catalyzed by the dehydrogenation of ammonia borane by platinum nanoparticles. Therefore, the successful preparation of platinum nanoparticles with high catalytic efficiency was significant. The assembly processes and morphology of dendritic Pt nanoparticles (DPNs) for different reaction time intervals were characterized by TEM. The one-

DOI: 10.1021/acs.analchem.9b03177
Anal. Chem. 2019, 91, 12055–12062

step produced DPNs followed an overgrowth mode. At the initial stage of the assembly process (3 min), the primary Pt NPs with an average dimension of 3 nm in diameter were formed according to reducing the precursor (Figure 2a). Then, primary Pt NPs step-by-step (5, 7 min) formed combined Pt NPs (Figure 2b, c), and further assemble (10 min) (Figure 2d, e) achieved dendritic platinum nanoparticles (DPNs), which were further validated by the corresponding selected-area electron diffraction (SAED) pattern (Figure 2g). Obviously, the coexistence of diffraction spots and diffraction rings for single DPN indicated that DPN was in a polycrystalline state. Moreover, DPN-catalyzing dehydrogenation of NH_3BH_3 to produce H_2 formed many bubbles (Figure 2i), while the NH_3BH_3 aqueous solution in the absence of DPNs (Figure 2h) did not form any bubbles. The specific process of DPNs catalyzing NH_3BH_3 to produce H_2 is shown in Figure 2f. Furthermore, DPNs labeled on the detection antibody were characterized by dynamic light scattering (DLS). The hydration diameter of Ab_2@DPNs (58 nm) was larger than those of pure DPNs (52 nm), indicating that DPNs were labeled on the detection antibody (Figure S2). DPNs containing a mass of Pt NPs from the overgrowth mode could catalyze the production of more hydrogen, resulting in a higher electrochemical response (Figure S3), demonstrating that DPNs still played the role of signal amplification compared with primary Pt NPs.

To explore the different response characteristics between Pd nanowires@ZIF-67 and a Pd nanowires sensing interface, low and high AFP concentrations were chosen for verification, respectively. As shown in Figure 2n, when the AFP concentration was at a relatively high concentration (50 ng mL^{-1}), correspondingly a high concentration of H_2 was produced by DPNs, and the response of the Pd nanowires sensing interface enhanced with increasing reaction time, gradually reaching a plateau. The response time of Pd nanowires was the time that the response increased up to $0.9R_{max}$ ($R = \Delta I/I_0$ (%)) and was sustained for 542 s. Once the Pd nanowires sensing interface was removed from the monitoring system and exposed to the air, the response returned to the initial state. Compared with Pd nanowires@ZIF-67 (16.99%) (Figure 2l), Pd nanowires (Figure 2n) had a higher response (18.40%) at the same reaction time (420 s). Nevertheless, Pd nanowires@ZIF-67 had superiority of a faster response time (134 s) to reach the plateau. Under a low AFP concentration condition (2.0 ng mL^{-1}), the produced low concentration H_2 reacting with Pd nanowires in the airtight detection device could extremely be affected by oxygen which occupied the majority of the adsorption site of hydrogen. Moreover, the chemisorbed O (Pd−O) reacted with adsorbed dihydrogen dissociating from hydrogen to generate water, causing a decrease in H absorption into PdH_x and a rapid decrease in sensing properties as well as poor responses of the Pd nanowires sensing interface (Figure 2m), which is as weak as the blank sample (Figure S3) at 2 ng mL^{-1}. On the other hand, the Pd nanowires@ZIF-67 could surmount the influence of oxygen owing to the interception of the ZIF-67 molecular sieve. The architecture networks built on the surface of Pd nanowires were connected with small apertures (3.31 Å) which could permeate H_2 (0.289 nm) and block O_2 (0.346 nm), leading to more PdH_x and a higher response of the Pd nanowires@ZIF-67 sensing interface (Figure 2k). Therefore, these results evidenced that H_2-based electrochemical biosensors utilizing Pd nanowires@ZIF-67 sensing interfaces, compared with Pd nanowires, were overwhelming whether in aspects of response value or response time for low AFP concentration detection.

Optimization of Experimental Conditions. The response effectiveness of the Pd nanowires@ZIF-67 sensing interface was further studied in the aspect of different self-assembly times (Figure 3a). The self-assembly time (1−6 h)

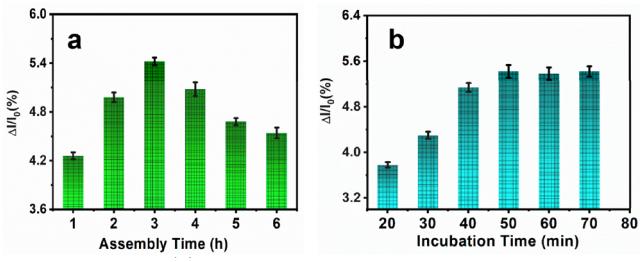

Figure 3. Effects of (a) ZIF-67 self-assembly time on the surface of Pd nanowires. (b) AFP and Ab_2@DPNs incubation times on H_2-based electrochemical biosensors (5.0 ng mL^{-1} AFP used in these cases).

had a significant influence on the response due to different coverage levels of ZIF-67 films. The response of the films assembled for 1 h was lower compared with longer assembly times because the low coverage of ZIF-67 was not enough for completely excluding the O_2 influence. Apparently, the 3 h assembly reached at the highest response and longer assembly time (4−6 h) was not favorable for optimum response due to the reduction of reaction sites of Pd NWs with the overgrowth of ZIF-67. In conclusion, 3 h of reaction time was chosen for ZIF-67 assembly to accomplish AFP detection in this strategy. Moreover, the incubation times for AFP and Ab_2@DPNs were considerable. As indicated in Figure 3b, the response increased with the increasing incubation time and remained a steady value after 50 min. A longer incubation time did not enhance the response of the Pd nanowires@ZIF-67 sensing interface. In order to save detection time, 50 min was utilized for the reaction between Ab_2@DPNs and target AFP (5.0 ng mL^{-1} AFP used in these cases).

Analytical Performance of H_2-Based Electrochemical Sensing Platform. To investigate the analytical performance of the developed H_2-based electrochemical biosensors, different concentrations of AFP standards were determined by Pd nanowires@ZIF-67 sensing interfaces in our strategy under optimum conditions. As seen from Figure 4a, the response was observed to gradually increase with the increasing target AFP concentration. A great linear relationship (Figure 4b) between the response and the AFP concentration was acquired within the dynamic range of 0.1−50 ng mL^{-1}. The linear regression equation was expressed as $\Delta I/I_0(\%) = 0.265\ C_{AFP} + 4.04$, ($R^2$ = 0.997, n = 7), where $\Delta I/I_0$(%) was the response of the H_2-based electrochemical biosensor toward different AFP concentrations. The limit of detection (LOD) was estimated to be 0.04 ng mL^{-1} ($3S_n/K$, where S_n stands for standard deviations (n = 11) in the blank sample, and K is the slope of the linear regression equation). Obviously, the LOD of this sensing strategy is comparable with those of commercial AFP ELISA kits from different companies, e.g., 0.5 ng mL^{-1} AFP from Abcam (cat# ab108838), 2.0 ng mL^{-1} AFP from Abcam (cat# ab108631), 0.0651 ng mL^{-1} AFP from Abcam (cat# ab193765), and 0.029 ng mL^{-1} AFP from R&D Systems (cat# MAFP00). The same comes true for the costs, i.e., ~US $1.021

DOI: 10.1021/acs.analchem.9b03177
Anal. Chem. 2019, 91, 12055−12062

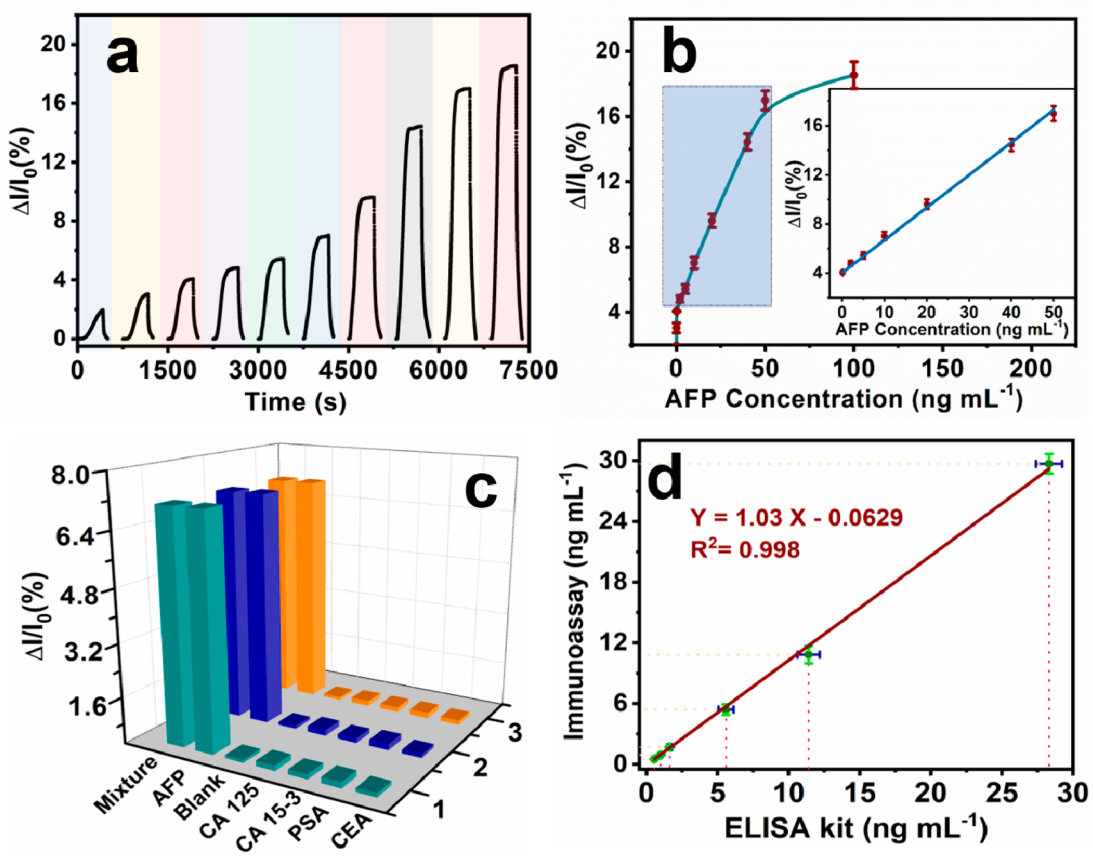

Figure 4. (a) Response ($\Delta I/I_0$) of H_2-based electrochemical biosensor toward different target AFP concentrations. (b) Corresponding linear relationship. (c) Selectivity of H_2-based electrochemical biosensor for 10 ng mL^{-1}AFP detection compared with other interfering proteins (concentrations of interfering proteins were 100 ng mL^{-1}) Note: The mixture contained the above-mentioned target AFP and nontargets. (d) Comparison of the results for the two methods.

and US $1.087 for a single test performed with a commercial ELISA test kit and the new strategy, respectively. Notably, this sensing system is capable of continuously carrying out all steps within 2 h per sample including the immunoreaction, washing, and electrochemical measurement, which was less than those of most existing commercialized AFP ELISA kits (~3.0 h).

The reproducibility of the reusable Pd nanowires@ZIF-67 sensing interface was also evaluated by AFP standards at different concentrations without repetitive interface assembly for 2 weeks. The final results (Figure S4) showed that the response of Pd nanowires@ZIF-67 films toward AFP standards at 2.0, 10, and 20 ng mL^{-1} maintained 91.6%−96.0% of their initial values, indicating acceptable reproducibility.

As for specificity of the H_2-based electrochemical biosensor, the sensing platform was studied by analyzing other possibly interferential biomarkers in human serum, such as cancer antigen 15−3 (CA 15−3), carcinoembryonic antigen (CEA), cancer antigen 125 (CA 125), and prostate specific antigen (PSA). In this case, we employed the concentration of interfering proteins at 10 times the concentration of the target AFP to explore their effects on the detection results. As displayed in Figure 4c, when the AFP was in the absence of detection system, the responses of four interferences were almost at the same level compared with the blank sample. In contrast, the response value of the mixture (including target AFP and interferential biomarkers) was approximately the same as the individual AFP response. Therefore, the H_2-based electrochemical biosensor had a satisfactory specificity for AFP detection.

The accuracy of the explored H_2-based electrochemical detection system was evaluated with a commercial AFP ELISA kit for AFP detection using six human serum specimens (collected from the local hospital). The final AFP concentrations monitored by two methods as well as t_{exp} values obtained from the Student's *t*-test method are listed in Table 1. The t_{exp} values in all cases were less than t_{crit} ($t_{crit[0.05,4]}$ = 2.77). As shown in Figure 4d, the regression equation between the two methods was calculated with $Y = 1.03X - 0.0629$ (R^2 = 0.998, n = 6), where the intercept and slope approached "0" and "1", respectively. All these results indicated no significant difference between the two methods. Therefore, the accuracy

Table 1. Comparison of Results Obtained from H_2-Based Electrochemical Immunoassay and Commercial Human AFP ELISA Kits for Human Serum Specimens

	method; conc. [mean ± SD (RSD), ng mL^{-1}, n = 3]		
sample	H_2-based immunoassay	AFP ELISA kit	t_{exp}
1	1.70 ± 0.1 (5.88%)	1.63 ± 0.15 (9.20%)	0.67
2	0.51 ± 0.04 (7.84%)	0.55 ± 0.02 (3.64%)	1.55
3	5.41 ± 0.51 (9.43%)	5.59 ± 0.53 (9.48%)	0.42
4	10.83 ± 0.86 (7.94%)	11.40 ± 0.78 (6.84%)	0.85
5	0.92 ± 0.06 (6.52%)	0.98 ± 0.04 (4.08%)	1.44
6	29.70 ± 0.97 (3.27%)	28.31 ± 0.92 (3.25%)	1.80

DOI: 10.1021/acs.analchem.9b03177
Anal. Chem. 2019, 91, 12055−12062

of the H_2-based electrochemical biosensor was acceptable for AFP detection.

CONCLUSIONS

In summary, H_2-based electrochemical biosensors with ZIF-67 molecular sieve-functionalized Pd nanowires sensing interfaces are developed for AFP detection. H_2 as a carrier of biological signals was produced by DPNs catalyzing dehydrogenation of NH_3BH_3. The corresponding electrochemical signals derive from the chemical signal transduction between the H_2 and Pd nanowires reaction. However, the presence of O_2 in the detection system restricts further response under low concentration AFP, which is surmounted by the molecular sieve function of ZIF-67 on the surface of Pd nanowires. Importantly, the H_2-based electrochemical biosensor achieves separating the sensing interface from the bioassembly platform. Compared with other detection schemes by using the biological assembly,[3,33−35] our strategy could efficiently avoid the reconstruction process of complex biological assembly on the sensing interface, thereby ensuring reproducibility and stability of the analysis results. Furthermore, DPNs assembled by vast small platinum nanoparticles could catalyze more dehydrogenation of NH_3BH_3, playing the role of signal amplification to achieve sensitive detection. Future work on MOF as a molecular sieve employed in electrochemical biosensors for the exploration of cancer biomarker detection should be focused on the enhancement of the sensitivity.

ASSOCIATED CONTENT

Supporting Information

The Supporting Information is available free of charge on the ACS Publications website at DOI: 10.1021/acs.analchem.9b03177.

Measurement with AFP ELISA kit for human serum samples, calculation method for *t*-test statistics, statistical analysis, and Figures S1−S5 (PDF)

AUTHOR INFORMATION

Corresponding Authors

*Phone: +86-591-2286 6125. Fax: +86-591-2286 6135. E-mail: dianping.tang@fzu.edu.cn (D. Tang).

*Fax: +49-89-2180 78255. E-mail: dietmar.knopp@ch.tum.de (D. Knopp).

ORCID

Dianping Tang: 0000-0002-0134-3983

Reinhard Niessner: 0000-0002-3781-0248

Dietmar Knopp: 0000-0003-4566-9798

Notes

The authors declare no competing financial interest.

ACKNOWLEDGMENTS

The authors acknowledged financial support from the National Natural Science Foundation of China (21675029, 201874022) and the Health-Education Joint Research Project of Fujian Province (WKJ2016-2-15).

REFERENCES

(1) Yu, Z.; Tang, Y.; Cai, G.; Ren, R.; Tang, D. *Anal. Chem.* **2019**, *91*, 1222−1226.

(2) Zeng, R.; Luo, Z.; Zhang, L.; Tang, D. *Anal. Chem.* **2018**, *90*, 12299−12306.

(3) Shu, J.; Qiu, Z.; Zhou, Q.; Tang, D. *Chem. Commun.* **2019**, *55*, 3262−3265.

(4) Zhang, J.; Liu, J.; Peng, Q.; Wang, X.; Li, Y. *Chem. Mater.* **2006**, *18*, 867−871.

(5) Li, Y.; Zu, B.; Guo, Y.; Li, K.; Zeng, H.; Dou, X. *Small* **2016**, *12*, 1420−1424.

(6) Song, C.; Yun, J.; Lee, H.; Park, H.; Jeong, Y.; Lee, G.; Kim, M.; Ha, J. *Adv. Funct. Mater.* **2019**, *29*, 1901996.

(7) Moon, W.; Yu, J.; Choi, G. *Sens. Actuators, B* **2002**, *87*, 464−470.

(8) Gao, M.; Cho, M.; Han, H.; Jung, Y.; Park, I. *Small* **2018**, *14*, 1703691.

(9) Koo, W.; Qiao, S.; Ogata, A.; Jha, G.; Jang, J.; Chen, V.; Kim, I.; Penner, R. *ACS Nano* **2017**, *11*, 9276−9285.

(10) Park, K. S.; Ni, Z.; Cote, A. P.; Choi, J. Y.; Huang, R.; Uribe-Romo, F. J.; Chae, H. K.; O'Keeffe, M.; Yaghi, O. M. *Proc. Natl. Acad. Sci. U. S. A.* **2006**, *103*, 10186−10191.

(11) Chen, J.; Chen, H.; Wang, T.; Li, J.; Wang, J.; Lu, X. *Anal. Chem.* **2019**, *91*, 4331−4336.

(12) Qin, L.; Wang, X.; Liu, Y.; Wei, H. *Anal. Chem.* **2018**, *90*, 9983−9989.

(13) Liu, G.; Cadiau, A.; Liu, Y.; Adil, K.; Chernikova, V.; Carja, I.; Belmabkhout, Y.; Karunakaran, M.; Shekhah, O.; Zhang, C.; Itta, A.; Yi, S.; Eddaoudi, M.; Koros, W. *Angew. Chem., Int. Ed.* **2018**, *57*, 14811−14816.

(14) Bux, H.; Liang, F.; Li, Y.; Cravillon, J.; Wiebcke, M.; Caro, J. *J. Am. Chem. Soc.* **2009**, *131*, 16000−16001.

(15) Hu, Y.; Wei, J.; Liang, Y.; Zhang, H.; Zhang, X.; Shen, W.; Wang, H. *Angew. Chem., Int. Ed.* **2016**, *55*, 2048−2052.

(16) Ban, Y.; Li, Z.; Li, Y.; Peng, Y.; Jin, H.; Jiao, W.; Guo, A.; Wang, P.; Yang, Q.; Zhong, C.; Yang, W. *Angew. Chem., Int. Ed.* **2015**, *54*, 15483−15487.

(17) Song, Z.; Qiu, F.; Zaia, E.; Wang, Z.; Kunz, M.; Guo, J.; Brady, M.; Mi, B.; Urban, J. *Nano Lett.* **2017**, *17*, 6752−6758.

(18) Krokidas, P.; Castier, M.; Moncho, S.; Sredojevic, D.; Brothers, E.; Kwon, H.; Jeong, H.; Lee, J.; Economou, I. *J. Phys. Chem. C* **2016**, *120*, 8116−8124.

(19) Knebel, A.; Wulfert-Holzmann, P.; Friebe, S.; Pavel, J.; Strauss, I.; Mundstock, A.; Steinbach, F.; Caro, J. *Chem. - Eur. J.* **2018**, *24*, 5728−5733.

(20) Shi, Q.; Chen, Z.; Song, Z.; Li, J.; Dong, J. *Angew. Chem., Int. Ed.* **2011**, *50*, 672−675.

(21) Kwon, H.; Jeong, H.; Lee, A.; An, H.; Lee, J. *J. Am. Chem. Soc.* **2015**, *137*, 12304−12311.

(22) Yamashita, T.; Forgues, M.; Wang, W.; Kim, J.; Ye, Q.; Jia, H.; Budhu, A.; Zanetti, K.; Chen, Y.; Qin, L.; Tang, Z.; Wang, X. *Cancer Res.* **2008**, *68*, 1451−1461.

(23) Wu, Y.; Guo, W.; Peng, W.; Zhao, Q.; Piao, J.; Zhang, B.; Wu, X.; Wang, H.; Gong, X.; Chang, J. *ACS Appl. Mater. Interfaces* **2017**, *9*, 9369−9377.

(24) Xu, D.; Liu, C.; Li, C.; Song, C.; Kang, Y.; Qi, C.; Lin, Y.; Pang, D.; Tang, H. *ACS Appl. Mater. Interfaces* **2017**, *9*, 37606−37614.

(25) Chen, W.; Ji, J.; Duan, X.; Qian, G.; Li, P.; Zhou, X.; Chen, D.; Yuan, W. *Chem. Commun.* **2014**, *50*, 2142−2144.

(26) Nyberg, C.; Tengstal, C. *J. Chem. Phys.* **1984**, *80*, 3463−3488.

(27) Huang, X.; Zheng, N. *J. Am. Chem. Soc.* **2009**, *131*, 4602−4603.

(28) Chen, X.; Liu, D.; Cao, G.; Tang, Y.; Wu, C. *ACS Appl. Mater. Interfaces* **2019**, *11*, 9374−9384.

(29) Wang, J.; Zhang, X.; Wang, Z.; Wang, L.; Xing, W.; Liu, X. *Nanoscale* **2012**, *4*, 1549−1552.

(30) Gao, Z.; Ye, H.; Tang, D.; Tao, J.; Habibi, S.; Minerick, A.; Tang, D.; Xia, X. *Nano Lett.* **2017**, *17*, 5572−5579.

(31) Qin, J.; Wang, S.; Wang, X. *Appl. Catal., B* **2017**, *209*, 476−482.

(32) Ren, R.; Cai, G.; Yu, Z.; Zeng, Y.; Tang, D. *Anal. Chem.* **2018**, *90*, 11099−11105.

(33) Shi, X.; Fan, G.; Shen, O.; Zhu, J. *ACS Appl. Mater. Interfaces* **2016**, *8*, 35091−35098.

(34) Chen, Y.; Guo, S.; Zhao, M.; Zhang, P.; Xin, Z.; Tao, J.; Bai, L. *Biosens. Bioelectron.* **2018**, *119*, 215−220.

DOI: 10.1021/acs.analchem.9b03177
Anal. Chem. 2019, 91, 12055−12062

(35) Da, H.; Liu, H.; Zheng, Y.; Yuan, R.; Chai, Y. *Biosens. Bioelectron.* **2018**, *101*, 213−218.

DOI: 10.1021/acs.analchem.9b03177
Anal. Chem. 2019, 91, 12055−12062